

Transport of Nanoparticles in Gases: Overview and Recent Advances

Lutz Mädler^{*}, Sheldon K. Friedlander[‡]

*Nanoparticle Technology and Air Quality Laboratory
Department of Chemical and Biomolecular Engineering, University of California,
Los Angeles (UCLA) 5819 Boelter Hall, Los Angeles, CA 90095 USA*

This paper is dedicated to Prof. emeritus Chiu-sen Wang, National Taiwan University, on the occasion of his 70th birthday

Abstract

Nanoparticles play a major role in industrial processes and natural phenomena in a variety of fields including chemical engineering, chemistry, physics, public health and biology. Nanoparticles are suspended in fluids during production, handling, processing, and by unintentional and/or undesirable release to the environment. In many cases the suspending fluid is a gas, as for example in large scale production, air pollution, clean room applications and many more. The small size of nanoparticles makes it possible to compare their transport properties to the fluid itself. Brownian particle diffusion is one of the most important mechanisms leading to significant transport rates. Diffusion is well known in mass transfer, however, differences arise because of the wide spectrum of nanoparticle sizes and their morphology (aggregate structure) – a concept understood in particle science and technology but needed in many diverse fields of nanoparticle applications. Nanoparticle transport can be controlled by external force fields because these forces may act exclusively on the nanoparticles and have negligible effects on fluid molecules. These include thermophoresis and forces in electrical fields.

Keywords: Nanoparticle; Thermophoresis; Transport; Diffusion.

[‡] deceased February 9, 2007

^{*} Corresponding author: Tel: +1-310-825 9926

E-mail address: lutz@seas.ucla.edu

Content

1. INTRODUCTION	306
1.1. Importance of nanoparticles and their transport.....	306
1.2. Nanoparticles in the environment	306
1.3. Engineered nanoparticles	307
1.4. Nanoparticle agglomerates.....	307
2. NANOPARTICLE TRANSPORT BY BROWNIAN DIFFUSION	309
2.1. Particle diffusivity	310
2.2. Continuum and free molecular approaches.....	315
2.3. Particle friction coefficient.....	316
2.4. Particle mean free path.....	320
2.5. Agglomerate diffusivity	321
2.6. Particle transport by Brownian diffusion: Conclusions	324
3. TRANSPORT OF NANOPARTICLES BY ADDITIONAL FORCES	325
3.1. Transport in temperature gradients	325
3.1.1. Thermal diffusion.....	326
3.1.2. Thermophoresis.....	326
3.1.2.1. Thermophoresis in the free molecular regime	327
3.1.2.2. Thermophoresis in the transition and continuum regime.....	328
3.1.2.3. Thermophoresis in the continuum regime: an alternative approach	330
3.1.2.4. Thermophoretic motion of agglomerates	332
3.1.2.5. Examples of technical applications of thermophoresis.....	333
3.2. Transport in electrical fields.....	335
3.2.1. Charging of nanoparticles	335
3.2.2. Transport of nanoparticles in an electrical field.....	336
4. NANOPARTICLE TRANSPORT IN CONVECTIVE FLOWS	337
5. SUMMARY	338
ACKNOWLEDGEMENT	338
REFERENCES	339

1. INTRODUCTION

1.1 Importance of nanoparticles and their transport

Nanoparticles play a major role in many industrial processes and natural phenomena in a variety of fields including chemical engineering, chemistry, physics, public health and biology. Nanoparticle technology is expected to have major impacts in medicine, catalysis, electronics and life science. Furthermore, science and engineering of nanoparticles is central to the environment (e.g. air pollution, climate change, and green house effect), energy utilization (e.g. fossil fuel combustion, and fly ash formation), and food engineering (e.g. flavor retention). Nanoparticles are suspended in fluids during production, handling, processing, and by unintentional and/or undesired release to the environment. In many cases the suspending fluid is a gas, as in the case of large scale commercial production (million tons of nanoparticles per year for fillers in rubber, opacifiers in paints etc.), air pollution (e.g. diesel emission and coal combustion), clean room applications (semiconductor industry) and many more. Gas properties such as viscosity and density are often not affected significantly because of the small size of nanoparticles and relatively low volume loading in gases, making classical fluid mechanics applicable. A key concept of the nanoparticle technologies with gases as the suspending fluids is the transport of nanoparticles and their deposition. Therefore, the subject can be addressed in the context of classical mass transfer approaches such as the analysis of Bird, Stewart, and Lightfoot (BSL) (2002), taking into account basic theoretical aspects addressed by Chandrasekhar (1943).

1.2 Nanoparticles in the environment

Particles in the size range from about 1 nm to 100 μm are present in trace quantities in the atmosphere. Particles smaller than 100 nm are also known as ultrafine particles. These nanoparticles play a central role in the formation of cloud droplets, precipitation, atmospheric visibility, ozone depletion in the stratosphere, and radiation balance of the earth (Wang *et al.*, 2005). In polluted air, the particle concentration can be higher than 10^4 per cm^3 being a major component that causes adverse effects on human health, materials, vegetation, and ecosystems (Seinfeld and Pandis, 1998). Particles from natural sources include those derived from biogenic, geogenic (soil dust, volcanic ash), oceanogenic (primarily sea sprays), and astrogenic (burning of falling meteoroids) sources. Examples of man-made ambient nanoparticles are emissions from industrial operations, farming, motor vehicles, ships, jet planes and solid fuel rockets. In these processes, nucleation and coagulation are major mechanisms in the formation and dynamics of nanoparticles. Both mechanisms involve mass transfer of either gaseous species or particles. Nucleation occurs when supersaturated vapors cool or when chemical reactions yield products of very low saturation vapor pressures. This leads to formation of stable nuclei and nanoparticles. Once such particles have been formed they collide due to their Brownian motion. Brownian

coagulation leads to the formation of larger particles and a decrease in the total particle number concentration. These mechanisms result in ambient ultrafine particles (nanoparticles) of different morphological properties and may be present as liquid droplets, compact solid particles, and agglomerates.

1.3 Engineered nanoparticles

Aerosol technology is an important route for the manufacture of commercial quantities of nanoparticles. Aerosol processes are based on the principle of gas-to-particle conversion, in which airborne particles are generated by homogeneous nucleation of a supersaturated vapor and subsequent growth by condensation and coagulation (Wang *et al.*, 2005). These mechanisms rely on mass transfer of the gas and the particles. In most cases diffusion of both phases (fluid and particles) is the dominant transport mechanism.

Commodity nanoparticle products are made by flame processes including carbon blacks (Cabot, Columbia, Degussa-Hüls, etc.), fumed silica (Cabot, Degussa-Hüls, etc.), pigmentary titania (DuPont, Ishihara, Millenium, Kerr-McGee, etc.) and optical fibers (Corning, Heraeus, Sumitomo, etc.). The annual production volume of the flame made nanoparticles is several million metric tons and typical production rates are of the order of 100 metric tons per day. The success and widespread application of this technology is based on its apparent simplicity of a one-step process and “no-moving parts” machinery (Kammler *et al.*, 2001). Aerosol processes are capable of producing a broad variety of materials with good control of product characteristics such as particle size, morphology, purity, chemical composition, and crystallinity (Kodas and Hampden-Smith, 1999; Wang *et al.*, 2005). Osterwalder *et al.* (2006) studied the economic and environmental parameters of aerosol processes in comparison with wet phase technologies. They have concluded that products with complex composition and most mixed oxide ceramics may be manufactured cheaper and environmentally friendlier by aerosol technology.

1.4 Nanoparticle agglomerates

Processes such as diesel combustion in car engines, flame synthesis, flame spray pyrolysis, or laser ablation lead to the formation of nanoparticle agglomerates. Agglomerates are three dimensional structures composed of primary particles (Fig. 1). The agglomerates result from collisions of compact (often spheroidal) primary particles or smaller agglomerates at temperatures sufficiently low to avoid complete coalescence before the next collision occurs (Bandyopadhyaya *et al.*, 2004). The resulting contacts between the primary particles may be of chemical nature (covalent and ionic bonding) resulting from neck formation between the nanoparticles. In this case the primary particles form hard agglomerates characterized by high particle – particle binding energies (Tsantilis and Pratsinis, 2004). Fig. 1a shows a transmission electron microscope (TEM) image of nanoparticles produced in a flame reactor. All nanoparticles

are present as agglomerates which have sintered necks between the primary particles when forming a hard agglomerate (Fig. 1b). The fractal like nature of agglomerates can be mathematically expressed through the statistical scaling law (Friedlander, 2000).

$$N_p = k_f \left(\frac{R_g}{d_p / 2} \right)^{D_f} \quad (1)$$

where N_p is the number of primary particles with diameter, d_p , that compose an agglomerate, k_f is the fractal prefactor, R_g is the radius of gyration, and D_f is the fractal dimension. The radius of gyration is defined as the mean root square of the distances between the spherule centers and the center of mass of the agglomerate. For compact agglomerates D_f is close to its maximum value of 3, while for chain-like structures D_f is close to 1 (see Fig. 2). Therefore, the fractal dimension is a measure of the agglomerate morphology which plays an important role in particle processing, transport and even health effects. Methods for measuring the fractal dimension have been summarized by Virtanen *et al.* (2004). Agglomerate formation occurs due to particle collisions (coagulation) and the fusion (formation chemical bonds) of particles in contact forming chemical bonds (sintering). Such mechanisms result in agglomerate structures with fractal dimension of about 1.8 (Friedlander, 2000) (Fig. 1b).

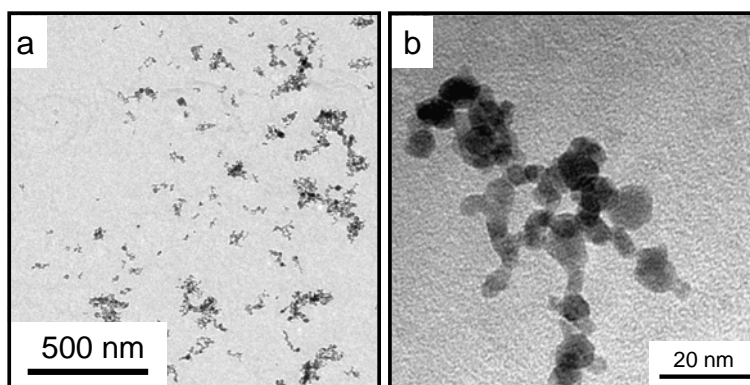


Fig. 1. (a) SnO_2 agglomerates synthesized by flame spray pyrolysis (FSP) (courtesy of ETH Zürich). The agglomerate formation occurs as a result of coagulation and subsequent sintering. Such mechanisms result in agglomerate structures with fractal dimension of about 1.8 (Friedlander, 2000). (b) Individual agglomerate showing single crystals connected by sintered necks forming a hard agglomerate with fractal dimension of 1.81.

Fig. 2 shows agglomerates generated by computer simulation with defined fractal dimensions and prefactors as described by Filippov *et al.* (2000). Agglomerates with fractal dimensions smaller than 2 (Fig. 2) can be defined as idealized agglomerates (Lall and Friedlander, 2006). Such agglomerates are “transparent”, that is, (nearly) all surfaces are directly exposed to collisions with molecules from the surrounding gas. For such agglomerates all primary particles are visible in the two dimensional projections enabling morphology and size analysis of these structures from TEM images (Rogak *et al.*, 1993). Fig. 2 also shows that the coordination number (the average number of contacts of a primary particle) of the aggregates with fractal dimensions smaller than 2 is only slightly larger two. Weber *et al.* (1997) have shown that silver aggregates with $D_f = 2$ have a coordination number of about 2.3. An increase in the fractal dimension above 2 results in an increase of the coordination number, for example $D_f = 3$ results in a coordination number of 5.4 (Weber and Friedlander, 1997).

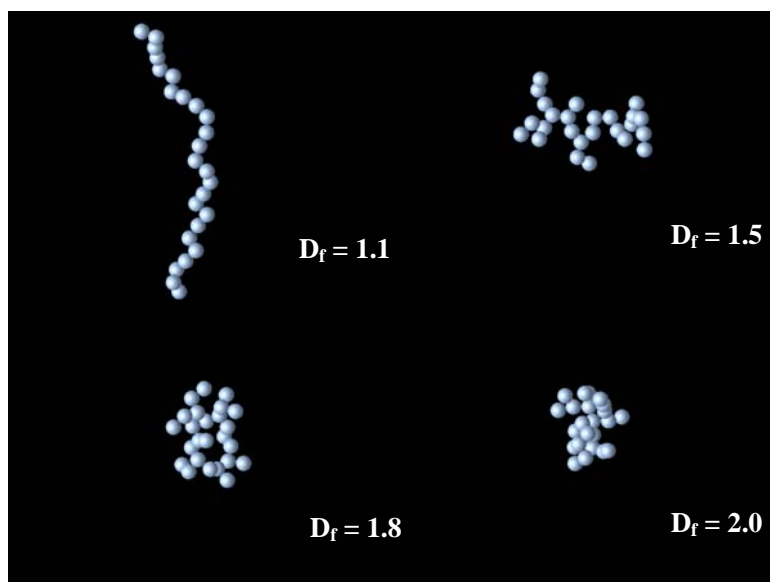


Fig. 2. Computer generated agglomerates with different fractal dimensions (D_f) and 25 primary particles (N_p). Larger fractal dimension results in more compact agglomerates (see Eq. 1).

2. NANOPARTICLE TRANSPORT BY BROWNIAN DIFFUSION

Brownian particle diffusion is one of the most important mechanisms leading to significant transport rates. Diffusion is well known in mass transfer of gases and liquids and included in chemical and mechanical engineering undergraduate curricula. However, diffusion of nanoparticles differs because of the wide spectrum of nanoparticle sizes and their morphology (aggregate structure) – a concept understood in particle science and technology but needed in many diverse fields of nanoparticle applications.

2.1 Particle diffusivity

We will start with a thought experiment: Imagine a flat surface tray which supports small metal balls (e.g. balls of a bearing) and a few larger metal rings (e.g. frames of a bearing). This tray is shaken parallel to the ground. The small balls will move very fast in straight lines until they hit another ball or the rim of the tray or a metal ring. The larger rings themselves will not move by the shaking because their inertia and drag on the tray is too large. However, hits by metal balls move the large rings slightly. If we keep shaking, the metal rings will perform a small wiggling motion due to the continuous random hits by the small metal balls. In 1827 the botanist Robert Brown studied the motion of small particles contained within pollen grains. He suspended these small particles in water and observed their wiggling motion under a light microscope (Brown, 1866). The smallest particles he studied were 0.8 micron. He noticed that the magnitude of the wiggling motion is much less for larger particles. Brown investigated different materials including inorganic minerals and found the wiggling motion for all of them. Brown also stated “these kinds of particles when immersed in water are generally seen in vivid motion; but the apparent motions of the larger particles might in these cases perhaps be caused by the rapid motion oscillation of the more numerous molecules.”, where the term “molecules” refers to the small particles. Today we know that his speculation was not far from the truth. The wiggling motion he observed is the particle diffusion that has its origin in the interaction with the thermal motion of the fluid molecules (the balls on our tray). To credit the observation of Brown, particle diffusion is also called Brownian diffusion. Brown’s experiment has been rebuilt in the Exploratorium - The museum of science, art and human perception at the Palace of Fine Arts, in San Francisco (<http://www.exploratorium.edu>).

We will start the derivation of the Brownian Diffusion with another thought experiment in which we assume that particles follow the same diffusion laws as molecules and their diffusivity can be described by a single parameter D . We will derive the particle diffusivity (D) later from first principles. In our experiment we release a monodisperse cloud of particles as a sharp pulse (Dirac’s delta function, $\delta(x)$) from a plane at $x = 0$. The initial high particle concentration (at $x = 0$ and $t = 0$) decays by diffusion into the x -directions (particles wiggle away from their original position). The problem is represented by the following differential equation following Fick’s second law:

$$\frac{\partial n}{\partial t} = D \frac{\partial^2 n}{\partial x^2}$$

where n is the one-dimensional (x coordinate) particle number concentration. The initial number of particles is n_0 at $t = 0$. The initial and boundary conditions are:

$$\begin{aligned} t = 0, \quad n &= n_0 \delta(x) \\ t > 0, \quad x &= \infty, \quad n = 0 \\ t > 0, \quad x = 0, \quad \frac{\partial n}{\partial x} &= 0 \end{aligned}$$

The solution has the form of Gaussian curve:

$$n(x, t) = \frac{n_0}{2\sqrt{\pi Dt}} \exp\left(-\frac{x^2}{4Dt}\right) \quad (2)$$

From Eq. (2) it can be readily shown that the average particle displacement is zero (the spatial distribution is centered at $x = 0$ for all t) because particle diffusion is isotropic (Fig. 3). However, the mean square displacement of the particles is non zero. The mean square displacement represents the spreading of the particle concentration (width of the distribution). The mean square displacement can be calculated as the second moment of the spatial distribution:

$$\overline{x^2} = \frac{1}{n_0} \int_{-\infty}^{+\infty} x^2 n(x, t) dx$$

which results in an integral of the form:

$$\int_{-\infty}^{+\infty} x^2 \exp(-a x^2) dx = \frac{1}{2a} \sqrt{\frac{\pi}{a}}$$

leading to the solution for the mean square displacement in one dimension:

$$\overline{x^2} = 2Dt \quad (3)$$

This is usually referred to as the Einstein equation and shows that the mean square displacement of a diffusing particle is proportional to the diffusion time. Eq. (3) is a very important expression which will be used to derive the particle diffusivity (D). It also enables first approximations about the distance particles are transported by diffusion during any time interval.

In what follows, the expression for the mean square displacement (Eq. 3) will be used to derive the particle diffusivity D from a force balance on a particle in Brownian motion (Chandrasekhar, 1943; Friedlander, 2000).

In one dimension this force balance has the form (BSL 17.5-1):

$$m \frac{du}{dt} = -F_D + F(t) = -\zeta u + F(t) \quad (4)$$

Where m is the mass of the particle, u its velocity, F_D is the drag force, $F(t)$ represents a fluctuating force and ζ is the friction coefficient. This fluctuating force results from the collision of the fluid molecules with the particle because the fluid molecules are in thermal motion (BSL 1.4-1). In this analysis the friction coefficient, ζ , is assumed to be independent of the particle velocity. Its dependence on particle size and shape and fluid properties will be discussed in detail in the next section.

Eq. (4) can be rearranged:

$$x \frac{du}{dt} + \beta u x = x A(t) \quad (5)$$

with the following definition:

$$\beta = \frac{\zeta}{m}; \quad A(t) = \frac{F(t)}{m}$$

and using the fact that:

$$\frac{d ux}{dt} = x \frac{du}{dt} + u \frac{dx}{dt} = x \frac{du}{dt} + u^2$$

Eq. (5) obtains the form:

$$\frac{d ux}{dt} + \beta ux = u^2 + A(t)x$$

which is a special case of the standard formula for ordinary differential equations:

$$\frac{d(ux)}{dt} + P(x)(ux) = Q(x)$$

with the following solution, where t' is a variable of integration representing time:

$$ux = \exp(-\beta t) \int_0^t u^2 \exp(\beta t') dt' + \exp(-\beta t) \int_0^t A(t') x \exp(\beta t') dt'$$

The term $\overline{A(t) \cdot x}$ is zero because there is no correlation between the displacement x and the “kick”, $A(t)$. The average of all particles:

$$\frac{(ux)_1 + (ux)_2 + \dots}{N_0} = \overline{ux}$$

leads to:

$$\overline{ux} = \frac{\overline{u^2}}{\beta} [1 - \exp(-\beta t)]$$

This expression can also be written as:

$$\overline{ux} = \frac{\overline{x dx}}{dt} = \frac{\overline{dx^2}}{2dt} = \frac{1}{2} \frac{\overline{dx^2}}{dt}$$

after integration the mean square displacement is obtained:

$$\frac{\overline{x^2}}{2} = \frac{\overline{u^2}}{\beta} t + \frac{\overline{u^2}}{\beta^2} [\exp(-\beta t) - 1]$$

For times much larger than the relaxation time of the particles

$$t \gg 1/\beta$$

one obtains, a direct relationship between the mean square displacement and the mean square velocity of the particle.

$$\frac{\overline{x^2}}{2} \approx \frac{\overline{u^2}}{\beta} t \quad (6)$$

The mean square velocity of the particle is directly related to its kinetic energy resulting from energy transfer of the gas molecules:

$$\frac{m \overline{u^2}}{2} = \frac{\kappa T}{2} \quad (7)$$

The left side of Eq. (7) represents the kinetic energy of the particle and the right side represents the translational energy of a gas molecule where κ is the Boltzmann constant. Combining Eqs. (3), (6) and (7) leads to an expression for the particle diffusion coefficient (Einstein, 1905):

$$D = \frac{\overline{x^2}}{2t} = \frac{\overline{u^2} t}{\beta t} = \frac{\overline{u^2} m}{\zeta} = \frac{\kappa T}{\zeta} \quad (8)$$

Eq. (8) is known as the Einstein relation and combines the properties of the fluid and the particle through the friction coefficient discussed in detail in the next chapters (Compare also to BSL 17.5-4).

Fig. 3 shows the final frame of a computer visualization for particle diffusion in one-dimensional space. Particles start to diffuse from a sharp pulse at $x = 0$ and each particle was subjected to a random displacement at each time step with a mean square displacement given by Eq. (3). The diffusion coefficient was calculated using Eqs. (8) and (12). The figure shows a frame representing 100 nm particles after their diffusion for 1 second. The particle positions are plotted in a histogram showing their Gaussian distribution as expected according to Eq. (2). Further graphs in Fig. 3 visualize the linear dependence of the particle mean square displacement variance on the diffusion coefficient and time, respectively, for different particle sizes.

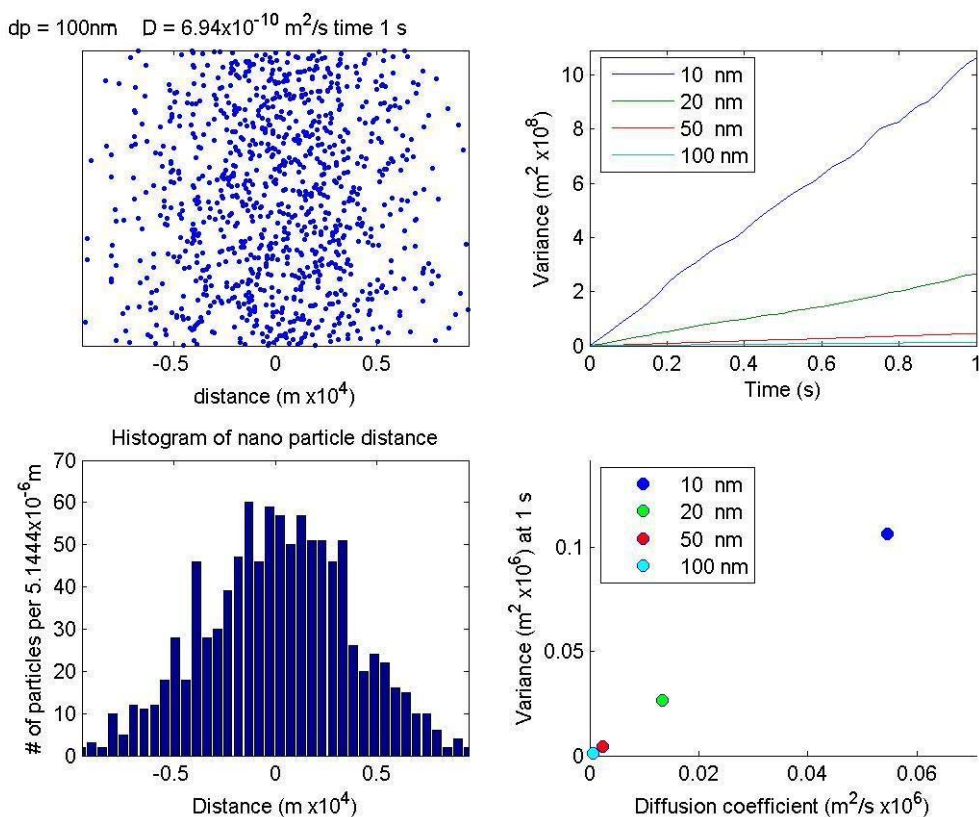


Fig. 3. Final frame of nanoparticle diffusion animation shown in upper left graph. The diffusion of spherical nanoparticles with diameters of 10, 20, 50 and 100 nm was visualized.

2.2 Continuum and free molecular approaches

Momentum, heat, and mass transfer between a particle and the surrounding gas molecules depend on the Knudsen number, Kn , which is the ratio of the mean free path of the gas molecules (ℓ_{gas}) (BSL 1.4-3, 9.3-3, 17.3-3) and the particle radius ($d_p/2$):

$$Kn = \frac{2 \ell_{gas}}{d_p}$$

The mean free path of the gas molecules (ℓ_{gas}) is the average distance a molecule travels before it changes its direction. The change in direction takes place when a gas molecule collides with another. The transfer processes follow continuum relationships at small Kn (large particles), but transfers to the free molecule regime at large Kn (small particles) (Wang *et al.*, 2005). Fig. 4 illustrates the different length scales for particle / gas interactions. The size of an air molecule (e.g. nitrogen) is about 0.3 nm. At standard conditions the average spatial distance between the gas molecules is about 3.3 nm. However, a gas molecule collides with another molecule after traveling about 65 nm because of their high mean velocity of about 470 m/s (BSL 1.4-1). Fig. 4

also shows a part of a 100 nm spherical particle. The corresponding Knudsen number for this example is 1.3. For nanoparticles at standard conditions, Kn is of the order of unity or larger.

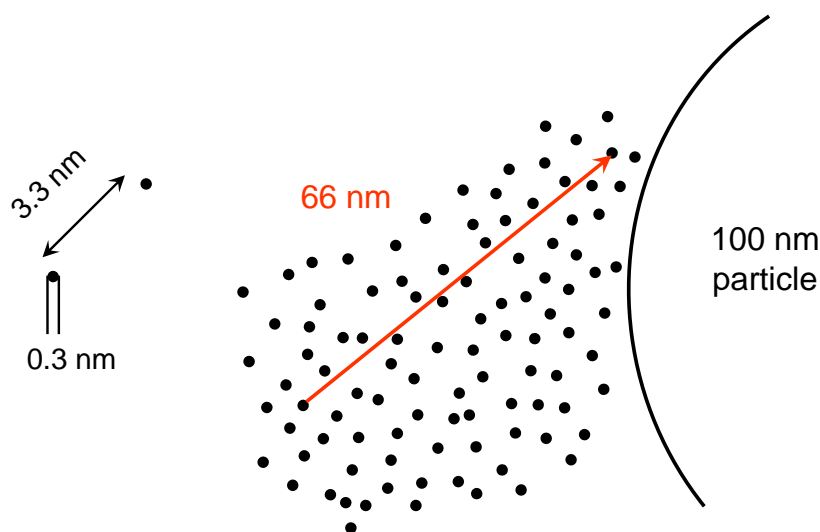


Fig. 4. Size of a gas molecule (0.3 nm, black circles) their average distance in space (3.3 nm), their mean free path (distance before collision, 66 nm) at standard conditions (arrow) in comparison with a 100 nm spherical particle (adapted from Hinds (1999)).

The mean free path of the gas molecules depends on pressure and temperature of the gas. The Knudsen number for a given particle can change significantly in non-isothermal environments such as aerosol reactors. The pressure and temperature dependence of the gas mean free path can be calculated as follows (Willeke, 1976):

$$\ell_{gas} = \ell_{gas,0} \left(\frac{T}{T_0} \right) \left(\frac{p_0}{p} \right) \left(\frac{1 + \frac{S}{T_0}}{1 + \frac{S}{T}} \right) \quad (9)$$

where $\ell_{gas,0} = 65.3$ nm is the mean free path of the gas molecules at conditions ($T_0 = 296$ K, $p_0 = 1$ atm) and S is the Sutherland constant ($S = 113$ K for air) which accounts for the attractive potential between the molecules (Chapman and Cowling, 1958).

2.3 Particle friction coefficient

The friction coefficient, ζ , is the proportionality constant between the drag force and the relative velocity between the particle and the fluid:

$$F_D = \zeta \cdot v \quad (10)$$

The friction coefficient combines fluid and particle properties (viscosity and particle size). In the Stokes regime ($Re \ll 1$) the friction coefficient for spherical particles has the following form:

$$\zeta = 3\pi \mu_B d_p \quad (11)$$

This equation is valid under the assumption that the relative velocity of the gas at the surface of the particle is zero. This assumption holds for particles much larger than the mean free path of the gas ($Kn \ll 1$). For smaller particles, a momentum “slip” exists at the surface which reduces their friction coefficient. This effect is taken into account by introducing the slip correction factor (also called Cunningham correction) C_c for spherical particles:

$$\zeta = \frac{3\pi \mu_B d_p}{C_c} \quad (12)$$

The slip correction factor is a function of the Knudsen number:

$$C_c = 1 + Kn \left(A_1 + A_2 \exp\left[\frac{-2A_3}{Kn}\right] \right) \quad (13)$$

The following parameters $A_1 = 1.257$, $A_2 = 0.40$, $A_3 = 0.55$ are often used (Davies, 1945), others have been proposed (Hinds, 1999).

In the limiting case of very small particles ($Kn \gg 1$) an expression for the friction coefficient can be derived from kinetic theory (Epstein, 1924):

$$\zeta = \frac{2}{3} d_p^2 \rho_B \sqrt{\frac{2\pi \kappa T}{m_B}} \left(1 + \frac{\pi \alpha}{8} \right) \quad (14)$$

where ρ_B is the gas density and m_B is the mass of the gas molecule. The accommodation coefficient α represents the fraction of gas molecules that are reflected diffusively and therefore leave the surface in equilibrium with the surface; $(1-\alpha)$ is the fraction of the molecules with specular reflection. This coefficient must be evaluated experimentally but is usually near 0.9 for momentum transfer (Friedlander, 2000). Recent theoretical studies suggest that the accommodation coefficient also depends on the Knudsen number (Li and Wang, 2003b). In

contrast to Stokes law, where the friction coefficient is proportional to d_p , it is proportional to d_p^2 in the free molecular regime (see Fig. 5 for detailed discussion).

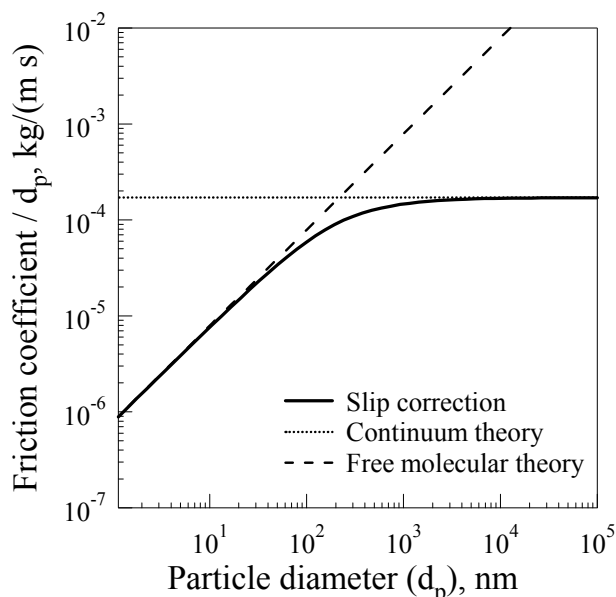


Fig. 5. Friction coefficient for spherical particles in the limiting cases of the free molecular regime (Eq. 14) and continuum regime (Eq. 11). The slip correction (Eq. 12) must be applied to particle diameters between 30 and 2000 nm at standard conditions (adapted from Li *et al.* (2003a)).

The case where the diffusing particles are in the same size range as the gas molecules is an important physical limit (very large Knudsen numbers). This limit should be carefully evaluated since $Kn \rightarrow \infty$ does not imply here that the mean free path becomes indefinitely large which would infringe the basic assumption of the ideal gas law (enough collisions per unit time from gas kinetic theory). In this limit ($Kn \rightarrow \infty$) we will show that under certain assumptions the Einstein relation is equivalent to the Chapman-Enskog equation. We start from the Einstein relation (Eq. 8 and BSL 17.5-4).

$$D_{AB} = \frac{\kappa T}{\zeta}$$

and apply the Epstein friction coefficient of the free molecular limit (Eq. 14):

$$\zeta = \frac{2}{3} d_p^2 \rho_B \sqrt{\frac{2\pi \kappa T}{m_B}} \left(1 + \frac{\pi \alpha}{8}\right)$$

Using the ideal gas law and introducing the Avogadro number, \tilde{N} , the mass diffusivity has the following form:

$$D_{AB} = \frac{1}{\left(\frac{2}{3}\left(1 + \frac{\pi \alpha}{8}\right)\sqrt{2\pi}\right)} \sqrt{(RT)^3 \frac{1}{M_B} \frac{1}{\tilde{N} d_p^2 p}} \quad (15)$$

Comparing Eq. (15) with the Chapman-Enskog equation (BSL 17.3-12) for mass diffusivity of binary mixture of nonpolar gases (low density):

$$D_{AB} = \frac{3}{16} \sqrt{\frac{2(RT)^3}{\pi} \left(\frac{1}{M_A} + \frac{1}{M_B}\right)} \frac{1}{\tilde{N} p \sigma_{AB}^2 \Omega_{AB}} \quad (16)$$

We further assume that the particle is a much larger “molecule” than the surrounding gas molecules and therefore $M_A \gg M_B$ and $\sigma_A \gg \sigma_B$. If we use the combination rule for the parameter σ_{AB} (BSL 17.3-15) and set $\sigma_A = d_p$, (which is a rather strong assumption as discussed later) Eq. (16) simplifies to

$$D_{AB} = 3 \sqrt{\frac{1}{8\pi} \frac{\sqrt{(RT)^3 \frac{1}{M_B}}}{\tilde{N} p d_p^2 \Omega_{AB}}} \quad (17)$$

Equating Eqs. (15) and (17):

$$3 \sqrt{\frac{1}{8\pi} \frac{\sqrt{(RT)^3 \frac{1}{M_B}}}{\tilde{N} p d_p^2 \Omega_{AB}}} = \frac{1}{\left(\frac{2}{3}\left(1 + \frac{\pi \alpha}{8}\right)\sqrt{2\pi}\right)} \sqrt{(RT)^3 \frac{1}{M_B} \frac{1}{\tilde{N} d_p^2 p}}$$

results in a simple relation between the collision integral Ω_{AB} and the accommodation coefficient α :

$$\Omega_{AB} = \left(1 + \frac{\pi \alpha}{8}\right)$$

In the case of specular reflection ($\alpha = 0$) Ω_{AB} approaches unity as in the case of non-interacting molecules. The connection between the Einstein relation and the Chapman-Enskog equation has been noted by Li and Wang (2003a). However, a more rigorous treatment of the comparison is given by Rudyak and Krasnolutski (2001), who derived the potential (Ω_{AB} , σ_{AB}) for the interaction of particles and molecules. They show also that the choice of the right potentials enables the extension of the Chapman-Enskog theory to particle diameters up to 10 nm in good agreement with the diffusion coefficient calculated from the Einstein relation using the slip correction (Eqs. 8 and 12).

2.4 Particle mean free path

The dynamic behavior of nanoparticles is different from that of gas molecules because they have a larger mass and therefore more inertia. When a molecule hits the particle, the particle velocity and direction persists to a large extent. Nevertheless, nanoparticles experience a change in direction during their Brownian motion. It takes more than one collision from the gas molecules to change the direction of a nanoparticle. However, molecular collisions are rather frequent (10^{12} per second for a 10 nm particle) and the change in direction occurs in short length scales. The distance a particle travels before it changes its direction (average length of a tangent to the trajectory from the point of contact to its intersection with the nearest perpendicular tangent (Fuchs, 1964) is defined as the particle mean free path. A schematic of this concept can be found elsewhere (Fuchs, 1964). It can be estimated considering the thermal motion of a particle in one direction (r) with the root mean square velocity:

$$\bar{v}_{p,rms,r} = \sqrt{\frac{\kappa T}{m_p}}$$

The particle will change its direction when the persistence of this velocity component vanishes. The time required for a particle to adjust or relax its velocity to a new condition of forces acting on the particle is called the relaxation time τ_p . The particle with the initial velocity component $\bar{v}_{p,rms,r}$ will relax in this direction for times larger than τ_p , which is related to the friction coefficient:

$$\tau_p = \frac{1}{\beta} = \frac{m_p}{\zeta}$$

The particle mean free path is defined as:

$$\ell_p = \bar{v}_{p,rms,r} \cdot \tau_p = \frac{\sqrt{m_p \kappa T}}{\zeta}. \quad (18)$$

The particle mean free path is an important length scale in particle deposition. In cases where diffusion is the dominant deposition mechanism, the particle mean free path can be larger than the particle diameter. This leads to ballistic deposition during the formation of nanoparticle deposits resulting in different structures of nanoparticle layers (Mädler *et al.*, 2006a). Fig. 6 shows the ratio of particle mean free path (Eq. 18) and the particle diameter over a large particle size spectrum from 1 to 1000 nm (particle density 1 g/cm³). The ratio decreases with increasing particle size. Nanoparticles smaller than about 30 nm persist in their direction and travel more than their own diameter in one direction. Particles larger than 30 nm change direction before they travel a distance corresponding to their own diameter.

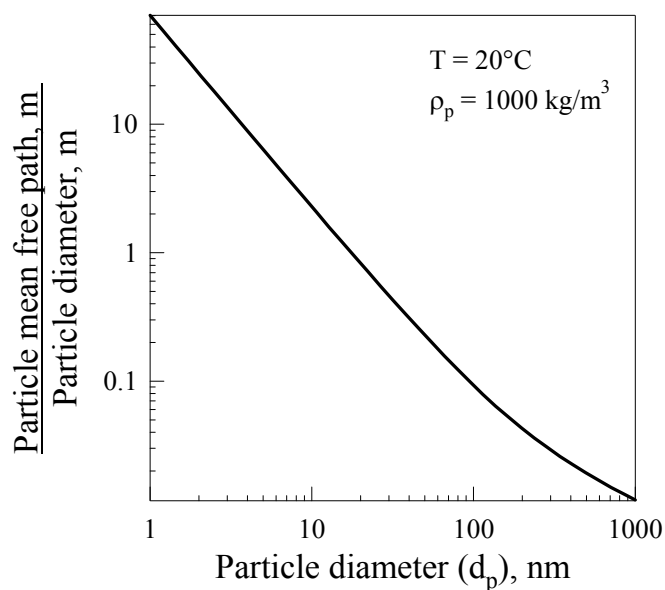


Fig. 6. Ratio of particle mean free path and particle diameter over a large particle size spectrum. Particles smaller than about 30 nm travel more than their own diameter before they change direction (partly adapted from Mädler *et al.* (2006a)).

2.5 Agglomerate diffusivity

The transport properties of nanoparticle agglomerates are important in many applications because agglomerates are the natural state of nanoparticles. To some extent their structure and properties can be compared to polymer chains. Diffusion of polymer chains in solvents has been

studied since the early 1950's. In the limit of dilute concentrations polymer diffusion depends on the extent of penetration of the solvent into the polymer chain. If the solvent fully penetrates the chain the Rouse theory can be applied (Rouse, 1953). In this case the friction coefficient of the chain can be approximated by the sum of the friction coefficients of the individual “beads” (primary particles) (ζ_p) (de Gennes, 1988):

$$\zeta_{agg} = \zeta_p \cdot N_p \quad (19)$$

If we apply these concepts to agglomerates suspended in gas, we find similar conditions for nanoparticle agglomerates in the free molecular regime. Agglomerates with fractal dimensions less than about two are “transparent”, that is, (nearly) all surfaces are directly exposed to collisions with molecules from the surrounding gas (Lall and Friedlander, 2006). These conditions apply to most of the agglomerates in the form of an aerosol.

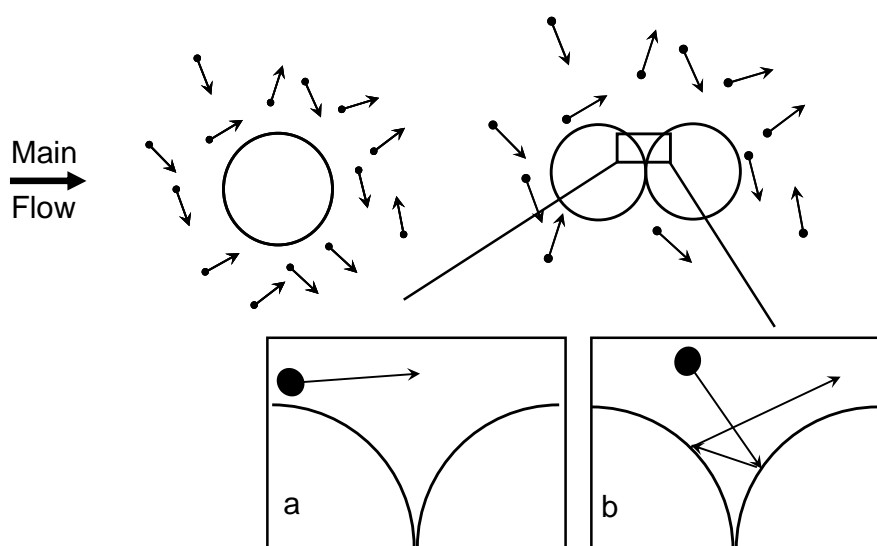


Fig. 7. Interaction of gas molecules with spherical particles and two connected spheres which are the basic chain units of agglomerates (see Fig. 2). For such concave shaped bodies, certain surface elements are not accessible to the gas molecules (a) and provide the possibility for more than one reflection (b) (Chan and Dahneke, 1981). This has a direct effect on the friction coefficient of agglomerates.

Chan and Dahneke (1981) computed in detail the drag on basic chain units (BCU) composed of two hemispheres with equal size (Fig. 7, here shown as two primary particles – double hemispheres) using a Monte Carlo method. The agglomerate friction coefficient, ζ_{agg} , in the free

molecular regime is obtained by adding the drag over all the BCU present in the chain agglomerate:

$$\zeta_{agg} = \frac{(c^*(N_p - 1) + c_{sph}^*) \mu_B d_p}{2 Kn} \quad (20)$$

where μ is the gas viscosity, N_p is the number of primary particles, c^* is the dimensionless drag of a basic chain unit and c_{sph}^* ($= 11.3$) is the dimensionless drag experienced by a single sphere, accounting for the presence of the two hemispherical end caps. Kn is defined with diameter of the primary particles. Therefore, the friction coefficient for spheres in the free molecular regime can also be expressed by:

$$\zeta_p = \frac{c_{sph}^* \mu_B d_p}{2 Kn}$$

which is equivalent to Eqs. (12) and (13) for $Kn \gg 1$. When the agglomerate orientation is random, the value of c^* is 9.34 for diffuse scattering of molecules and 6.85 for specular scattering of molecules. Dahneke (1982) assumed 7% specular reflection and 93% diffuse reflection to calculate the friction coefficient. This leads to $c^* = 9.17$ for agglomerates with statistically averaged orientation. Lall and Friedlander (2006) developed the idealized aggregates (IA) theory for calculations of the agglomerate friction coefficient.

Fig. 8 compares calculated agglomerate diffusion coefficients in the free molecular regime for different numbers of primary particles. The agglomerates are composed of primary particles with a diameter of 10 nm. The analysis of Chan and Dahneke and Lall and Friedlander (1981; 2006) (bold solid line) and the rather simple theory by Rouse (1953) (dotted line) differ only by about 20% for $N_p = 100$. This results from the c_{sph}^*/c^* - ratio ($11.3/9.34 = 1.21$) for primary particles in the free molecular regime. However, approximating the agglomerate by its volume equivalent sphere ($= d_p (N_p)^{1/3}$) leads to a considerable difference by more than a factor of four for $N_p = 100$ (thin solid line). The hydrodynamic drag of agglomerates with fractal dimensions of $D_f = 1.7 - 2.0$ in the free-molecular regime was studied in detail by Mackowski (2006) using a Monte Carlo method. The results indicated that the fractal parameters D_f and k_f (Eq. 1) have relatively small effect on the agglomerate drag. The empirical interpolation formula proposed by Mackowski (2006) is used to calculate the diffusion coefficient for agglomerates with $D_f = 1.8$ (Fig. 8, short dashed line). For $N_p=100$ the diffusion coefficient is less than 35% larger than predicted by Chan and Dahneke and Lall and Friedlander (1981; 2006). Fig. 8 also shows that agglomerate diffusion

models based on the radius of gyration (Eqs. 1, 8 and 12) are not applicable (long dashed line). For fractal dimensions larger than two and larger primary particles (continuum regime) the fractal dimension may be an important parameter to consider (Tandon and Rosner, 1995). This may also be equivalent to polymer diffusion where the diffusion coefficient is proportional to the radius of gyration for non-penetrating (not transparent) chains (Kirkwood and Riseman, 1948).

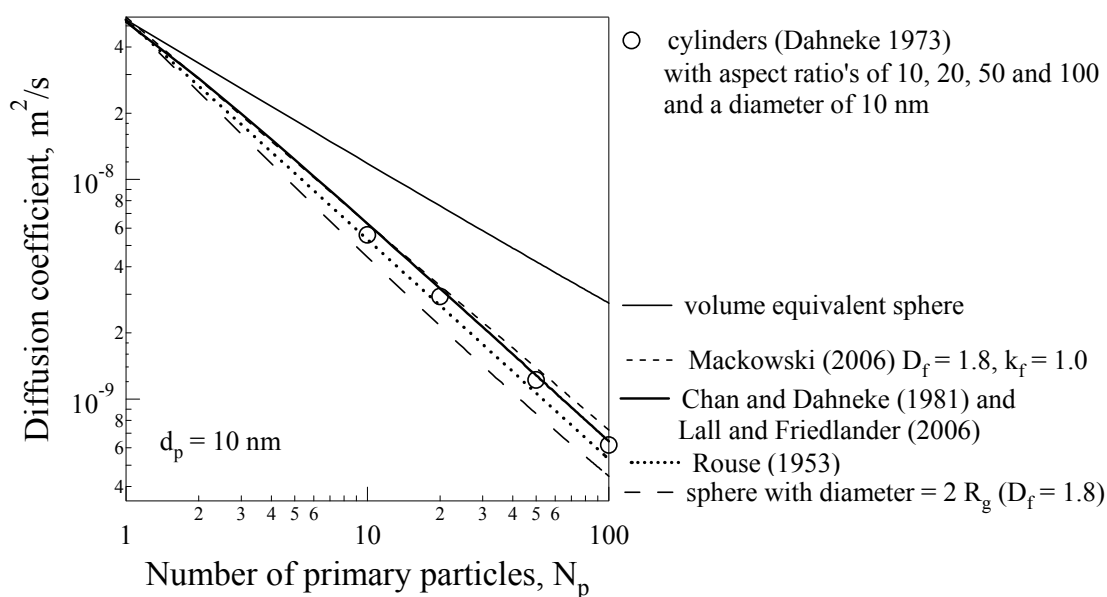


Fig. 8. Agglomerate diffusion coefficients (primary particle diameter is 10 nm) at standard conditions calculated under the following assumptions: diffusion of agglomerate is equal to volume equivalent sphere (Eqs. 8 and 12) (thin solid line); empirical interpolation formula of Mackowski (2006) for $D_f = 1.8$ (short dashed line); theory of Chan and Dahneke and Lall and Friedlander (1981; 2006) (Eqs. 8 and 20) (thick solid line); theory of Rouse (1953) (Eqs. 8 and 19) (dotted line); sphere with the diameter of gyration of the agglomerate for $D_f = 1.8$ (Eqs. 1, 8 and 12) (long dashed line). For comparison the diffusion coefficients of random oriented cylinders (cylinder diameter is 10 nm) with aspect ratios of 10, 20, 50 and 100 are also shown (symbols) (Dahneke, 1973).

2.6 Particle transport by Brownian diffusion: Conclusions

Diffusion is one of the main transport mechanisms of nanoparticles in gases in quiescent air in the absence of external forces. Fig. 9 shows the root mean square displacement (Eq. 3) of spheres with different diameters after diffusing 1 second (Eqs. 8 and 12). More than one third of all particles traveled at least that distance from their original position during that time interval which can be seen from the Gaussian curve represented by Eq. 2. A 10 nm particle has traveled more than ten thousand times its own diameter. Fig. 9 also shows the strong size dependence of the particle diffusivity.

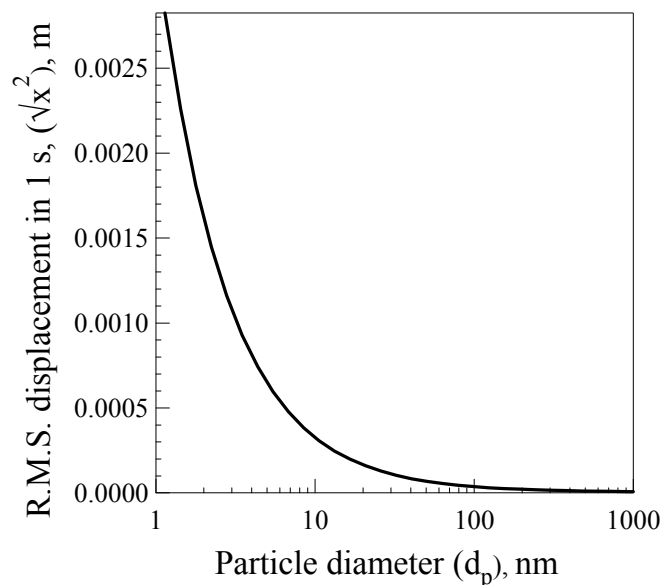


Fig. 9. Root mean square displacement of spherical particles after 1 second of Brownian diffusion (Eqs. 8 and 12). Transport by Brownian diffusion is important for particles smaller than about 500 nm.

In an aerosol the diffusive motion of the particles leads to particle – particle collisions. Most of the collisions result in strong particle – particle interactions or even coalescence. This process is known as Brownian coagulation. For nanoparticles suspended in a gas Brownian coagulation has by far the highest collision rates compared with other transport mechanisms (e.g. turbulent flow) (Friedlander, 2000).

Nanoparticle diffusion is also an important mechanism for deposition in filter media or in the lung. In the lung, Brownian motion is the dominant deposition mechanism during pause between the inhalation and exhalation (Wang *et al.*, 2005).

3. TRANSPORT OF NANOPARTICLES BY ADDITIONAL FORCES

Nanoparticle transport can be controlled by external force fields because these forces may act primarily on the nanoparticles and have negligible effects on fluid molecules. In this chapter we consider the forces on nanoparticles due to temperature gradients and electric fields.

3.1 Transport in temperature gradients

Temperature gradients can lead to the transport of molecules and nanoparticles. While the first mechanism is called thermal diffusion, the second is called thermophoresis. After a short introduction to thermal diffusion, thermophoresis is discussed in detail.

3.1.1 Thermal diffusion

In a stationary vessel containing a gas mixture a constant temperature gradient can produce a concentration gradient of the gas components. This transport of mass is called thermal diffusion. In the late 1930's a process combining convection and thermal diffusion was described, by which mixtures of gases, particularly of isotopes, can be separated (Chapman and Cowling, 1958). The invention enabled the enrichment of radioactive material. Today, because of their high energy requirements thermal diffusion processes have been replaced by centrifugation for separation of isotopes. Thermal diffusion is characterized by the thermal diffusion ratio, k_T . It is a measure of the relative importance of thermal (D^T) and the mass (D) diffusivity (Hirschfelder *et al.*, 1964):

$$k_T = \frac{\rho}{n^2 m_1 m_2} \frac{D_A^T}{D_{AB}}$$

where n is the number density of all molecules and m_1, m_2 are the masses of the gas molecules. The concentration gradient formed by a temperature gradient at steady state is given by (Hirschfelder *et al.*, 1964):

$$\frac{\partial}{\partial r} \left(\frac{n_1}{n} \right) = -k_T \frac{\partial}{\partial r} \ln T$$

The thermal diffusion ratio, k_T , is a complex function of temperature, concentration and molecular weights of the gases in the mixture. It becomes effective for large differences in molecular weights of the gas molecules and reduces to zero for equal molecular weights (Hirschfelder *et al.*, 1964). The thermal diffusion ratio can be positive or negative depending on the average temperature within the temperature gradient (Hirschfelder *et al.*, 1964) and on the concentration (Chapman and Cowling, 1958). Values of k_T are in the order of 10^{-2} (Hirschfelder *et al.*, 1964).

3.1.2 Thermophoresis

Thermophoresis is an important nanoparticle transport mechanism with many applications in aerosol technology (Zheng, 2002). Thermophoresis describes particle motion due to a temperature gradient in the surrounding fluid. This effect was first reported by Tyndall (1870). He noticed a particle free region around a heated metal wire which was visible as a dark space in the bright background of scattered light from the particles (“When the wire is white hot, it sends up a band of intense darkness”). Today, thermophoresis is used to remove small particles from gas streams in precipitators (Gleiter, 1989), as an aerosol sampling method (Dobbins and Megaridis, 1987), as a deposition method for nanoparticle film manufacture (Mädler *et al.*, 2006b)

and for light guide production (Simpkins *et al.*, 1979). The semiconductor industry uses thermophoresis to avoid “Light Point Defects” on wafers and lithographic masks by particle deposition (Stratmann *et al.*, 1988; Peterson *et al.*, 1989; Ye *et al.*, 1991). Thermophoresis also causes undesired effects such as particle loss in aerosol furnace reactors (Weimer *et al.*, 1993; Walsh *et al.*, 2006). Thermophoretic particle deposition in boilers and heat exchangers results in scale formation and reduction in heat transfer (Kaer *et al.*, 2006). It also contributes to particle deposition on paintings in galleries and museums (Nazaroff *et al.*, 1990).

3.1.2.1 Thermophoresis in the free molecular regime

In the free molecular regime ($Kn \gg 1$) particle transport towards the lower temperature zone results from the bombardment of molecules with higher energy in the hotter zone (see Fig. 10 for detailed description).

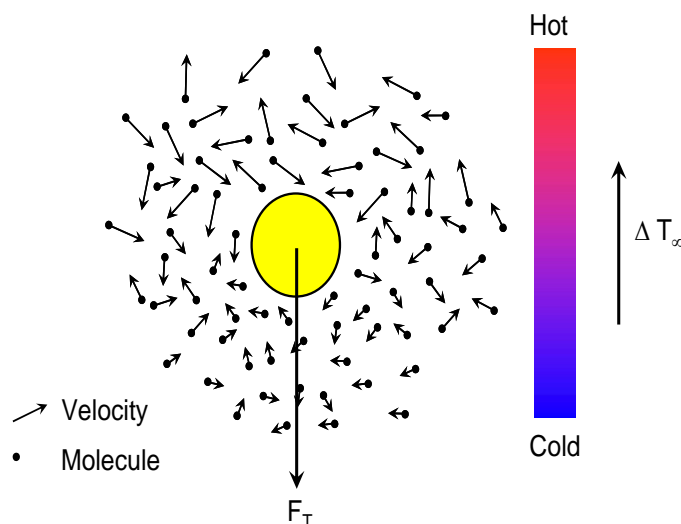


Fig. 10. Schematic diagram of a particle (large center sphere) immersed in a gas. The small black dots represent the gas molecules which are randomly fluctuating. Their velocity is a function of the gas temperature (BSL 1.4-1) indicated as vector arrows. In a temperature gradient the mean velocity of the gas molecules also has a gradient. Momentum is transferred upon collision of the gas molecules with the particle. The momentum transfer is a function of the gas molecule velocity. The gradient in the mean molecular velocities produces a force on the particle and a particle movement against the temperature gradient towards the colder region (adapted from Zheng (2002)).

Waldmann *et al.* (1966) calculated the particle thermophoretic force from the kinetic theory of gases. Their original formula can be rearranged by substituting the mean speed of the gas molecules:

$$F_{th} = -\frac{4\sqrt{\pi}}{15} d_p^2 \frac{k_g \nabla T}{\sqrt{\frac{2\kappa T}{m_B}}} \quad (21)$$

The factor k_g represents the thermal conductivity of the gas which can be expressed by the following relation according to (BSL 9.3-14):

$$k_g = \frac{15 \kappa \mu_B}{4 m_B} \quad (22)$$

The thermophoretic velocity in the free molecular regime is calculated by equating the thermophoretic force (Eqs. 21, 22) to the drag force (Eqs. 10, 14):

$$v_{th} = -\frac{3 \mu_B}{4 \rho_B \left(1 + \frac{\pi \alpha}{8}\right)} \frac{\nabla T}{T} \quad (23)$$

According to Eq. (23) the thermophoretic velocity of particles in the free molecular regime does not depend on particle size and composition. However, for small nanoparticles (5 nm and less) the accommodation coefficient α may depend on these particle parameters (Li and Wang, 2003a).

Recently, the thermophoretic force on spherical particles in the free molecular regime has been predicted using the momentum transfer method coupled with molecular velocity distribution functions calculated by the direct simulation Monte Carlo (DSMC) method (Gallis *et al.*, 2001). These methods have shown that the model of Waldmann *et al.* (1966) can be used with acceptable accuracy to calculate the thermophoretic force on particles in monoatomic and polyatomic gases and their mixtures. Advantages of DSMC models are the ability to consider wall effect and any given gas mixture (Gallis *et al.*, 2004).

3.2.1.2 Thermophoresis in the transition and continuum regime

For particles that are larger than the mean free path of the gas, the motion in a temperature gradient is rather difficult to describe theoretically. The explanation is based on a creep velocity directed towards the high temperature side, propelling the particle towards the low temperature side. Brock (1962) derived the thermophoretic velocity in the continuum regime using a fluid mechanics approach with slip-corrected boundary conditions. The thermophoretic force given by

Brock (1962) is a function of thermal (C_t) and momentum (C_m) exchange coefficients which can be expressed by the accommodation coefficient (α) (Ivchenko *et al.*, 1971; Talbot *et al.*, 1980):

$$F_{th} = -\frac{9}{2} \pi \frac{\mu_B^2}{\rho_B} d_p \left(\frac{1}{1+3C_m Kn} \right) \left(\frac{\frac{kg}{kp} + C_t Kn}{1+2\frac{kg}{kp} + 2C_t Kn} \right) \frac{\nabla T}{T}$$

Best agreement with experimental data was obtained with $C_t = 2.48$ and $C_m = 1.00$ for pure diffuse reflection of molecules. Equating the thermophoretic force with the particle drag force (Eqs. 10, 12) results in the thermophoretic velocity (Brock, 1962):

$$v_{th} = -\frac{3}{2} \frac{\mu_B}{\rho_B} C_c \left(\frac{1}{1+3C_m Kn} \right) \left(\frac{\frac{kg}{kp} + C_t Kn}{1+2\frac{kg}{kp} + 2C_t Kn} \right) \frac{\nabla T}{T} \quad (24)$$

It can be shown that in the limit of $Kn \rightarrow \infty$ the thermophoretic velocity given by Eq. (24) is 57% of the thermophoretic velocity in the free molecular regime derived by Waldmann (1966) (Eq. 23) when approximating the Cunningham correction factor by $C_c = (1 + 1.257 Kn)$ (Eq. 13). This enabled the interpolation of the original equation by Brock (1962) from the continuum to the free molecular regime (Fig. 11). Talbot *et al.* (1980) suggested the following relation:

$$F_{th} = -6 \pi \frac{\mu_B}{\rho_B} d_p C_s \left(\frac{1}{1+3C_m Kn} \right) \left(\frac{\frac{kg}{kp} + C_t Kn}{1+2\frac{kg}{kp} + 2C_t Kn} \right) \frac{\nabla T}{T}$$

The dimensionless coefficients C_m and C_t are manifestations of non-continuum hydrodynamic isothermal ‘‘velocity slip’’ and ‘‘thermal jump’’ effects, respectively, whereas C_s is Maxwell’s, non-isothermal slip-velocity (thermal creep) coefficient which can also be expressed as a function of the accommodation coefficient α . The thermophoretic velocity is derived by equating the thermophoretic and drag force using Eqs. (10, 12):

$$v_{th} = -\frac{2\mu_B C_s \left(\frac{kg}{kp} + C_t Kn \right) C_c}{\rho_B (1+3C_m Kn) \left(1+2\frac{kg}{kp} + 2C_t Kn \right)} \frac{\nabla T}{T} \quad (25)$$

A compilation is available of ‘‘best fit’’ experimental values for these three semi-empirical coefficients, corresponding to the values $C_s = 1.17$, $C_m = 1.14$ and $C_t = 2.18$.

3.2.1.3 Thermophoresis in the continuum regime: an alternative approach

Despite the wide acceptance that the velocity appearing in Newton's viscosity law is the mass average velocity (BSL B.6 and 17.7-1):

$$\mathbf{v} = \mathbf{v}_m$$

Brenner (2005b) proposed that volume average velocity, \mathbf{v}_v :

$$\mathbf{v} = \mathbf{v}_v$$

would be a better representation in some cases. In an isobaric compressible system, temperature gradients within a fluid element result also in a density gradient (e.g. ideal gas law). Such a density gradient leads to fluid motion with regard to the volume of the fluid. Particles that are embedded in the moving compressible fluid parcel will be transported as a result of the density and therefore temperature gradient. This analysis is especially helpful in the continuum regime where the discussion based on molecular gas dynamics cannot be applied readily. In what follows we will introduce the analysis of Brenner (2005b) and compare it to the experimentally based results of Talbot *et al.* (1980) (Eq. 25).

The volume and mass velocities are related through the diffusion velocity of volume (compare to BSL 17.7-3 and -4) (called diffusive flux by Brenner (2005b))

$$\mathbf{v}_v = \mathbf{v}_m + \mathbf{j}_v. \quad (26)$$

The derivation of the diffusion velocity has been given in detail by Brenner (2005a):

$$\mathbf{j}_v = \alpha_v \nabla \ln \rho_B, \quad (27)$$

where α_v is the volume diffusivity defined by Brenner (2005a). For ideal gases the temperature is inversely related to the density and therefore the diffusion velocity becomes positive with regard to the density gradient (Eq. 27). The respective heat or mass-transfer cases to which Eq. (27) can be applied corresponding to $\rho_B = \rho_B(T)$ for a fixed pressure. In case of an incompressible fluid the fluid density, ρ_B , is uniform throughout the fluid and the mass and volume velocities are equal.

In this framework the velocity of the solid particle \mathbf{u} , at a point lying on its surface ∂V_s is:

$$\mathbf{v}_v - \mathbf{u} = 0 \quad \text{on} \quad \partial V_s \quad \text{for a non-conducting sphere}$$

since $\mathbf{v}_m = 0$ in a quiescent fluid it follows from Eq. (26) that

$$v_v = j_v = u \quad (28)$$

The particle velocity (u) is equal to the volume velocity because the density gradient is coupled to it. This links the particle's thermophoretic motion to the fluid's thermal expansion.

More specifically using the fluid coefficient of thermal expansion, β_{th} at constant pressure:

$$\beta_{th} = - \left(\frac{\partial \ln \rho_B}{\partial T} \right)_p \quad (29)$$

the particle velocity can be expressed for non-conducting spheres using Eqs. (27, 28, 29):

$$U = v_{th} = - \alpha_v \beta_{th} \nabla T$$

A more detailed calculation for the case $k_p \neq 0$ yields (Brenner, 2005b):

$$u = v_{th} = - \frac{\alpha_v \beta_{th}}{1 + (k_p / 2k_g)} \nabla T$$

The volume diffusivity for gases is related to the Prandtl number, Pr, by the following relation (BSL Eq. 9.3-16):

$$\alpha_v = \frac{1}{Pr} \frac{\mu}{\rho}$$

where $Pr = c_p \mu / k_g$. Using the fact that $\beta_{th} = 1/T$ for ideal gases, we obtain:

$$u = v_{th} = - \frac{1}{Pr} \frac{1}{1 + (k_p / 2k_g)} \frac{\mu}{\rho} \frac{\nabla T}{T} \quad (30)$$

In the continuum regime ($Kn = 0$) with $Pr \approx 0.73$ for a di-atomic gas (Table for Pr is given in BSL 9.3-1) this relation predicts a thermophoretic velocity which is only 17% higher from the empirical correlation of Talbot *et al.* (1980) (Eq. 25). Eq. (30) is based upon purely continuum-mechanical arguments (without slip), which suppose that $v = v_v$. In summary, Brenner identifies

the density gradient to be the fundamental source of the velocity difference for thermophoretic particle motion in the continuum regime.

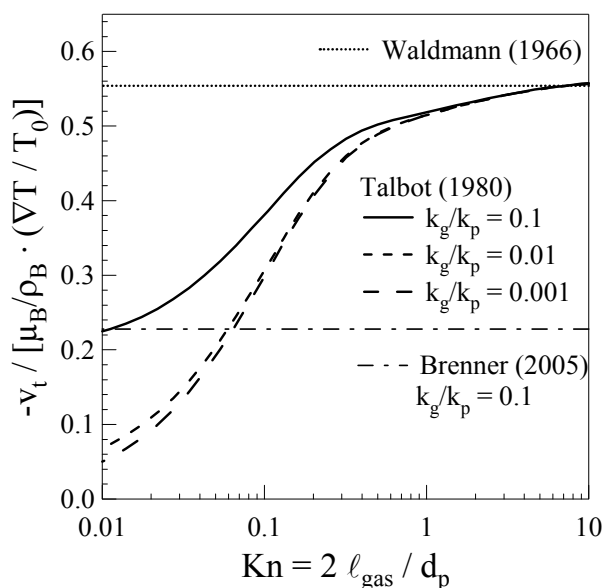


Fig. 11. Dimensionless thermophoretic velocity calculated based on the relations of Waldmann and Schmitt (1966), Eq. (23); Talbot *et al.* (1980), Eq. (25); and Brenner (2005b), Eq. (30). For $\text{Kn} > 1$ (particles smaller than the mean free path) the velocity becomes independent of particle composition and size. In this limit the equation derived by Waldmann (1966) for the free molecular limit can be used. For smaller Knudsen numbers (particles larger than the mean free path) the thermal conductivity ratio between the particle and the gas (k_g/k_p) becomes an important factor. High particle conductivity results in a decrease of the temperature gradient around the particle by thermal conduction within the particle. For particles in the continuum regime $\text{Kn} \ll 1$ the thermophoretic velocity becomes independent of particle size as predicted by Brenner (2005b) and (Talbot *et al.*, 1980) (Fig. adapted from Friedlander, 2000).

3.1.2.4 Thermophoretic motion of agglomerates

Mackowski (2006) and Zurita-Gotor (2006) independently stated that for nanoparticle agglomerates ($\text{Kn} > 1$, $D_f < 2$) the thermophoretic velocity is independent of size and morphology. In the transition regime Mackowski (2006) has theoretically shown that the thermophoretic velocity of agglomerates obeying the IA theory with random orientation is only slightly larger than that of spherical particles with the same volume. In the near-continuum regime thermophoresis can result in an orienting torque on the agglomerate (Mackowski, 1990) which for sufficiently large temperature gradients offset the randomizing action of Brownian rotation (Filippov, 2001). In addition, thermal nonequilibrium caused by particle radiation absorption and/or emission can result in body-fixed phoretic forces which can be considerably larger than the space-fixed forces arising from thermophoresis.

3.1.2.5 Examples of technical applications of thermophoresis

Fabrication of optical fibers

Optical fibers for today's telecommunication are produced in a modified chemical vapor deposition (MCVD) process in which a high temperature stream carrying silica-germanium particles (about 10 nm or larger) deposit on the inner wall of the optical fiber preform tube (Fig. 12) (Simpkins *et al.*, 1979). In this process thermophoresis is the dominant effect by which silica and germania particles deposit on the wall in the MCVD process while the gas flow is parallel to the tube wall (left to right in Fig. 12). Understanding of the thermophoretic principles has led to better design of the process and higher deposition rates by establishing a radial temperature gradient around the fiber preform. After the deposition process is completed the preform is calcined to an optical fiber.

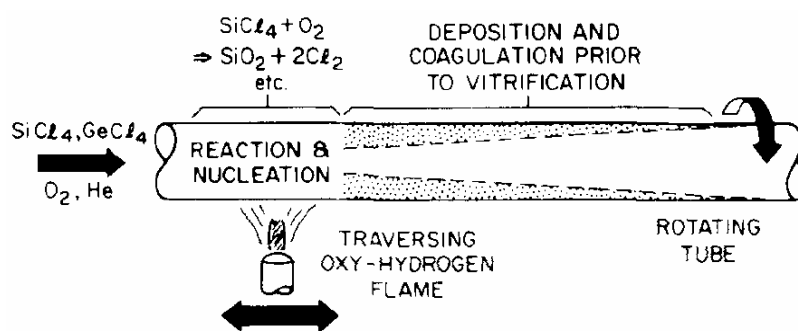


Fig. 12. Schematic of particle deposition in the fabrication of optical light guide preforms (Simpkins *et al.*, 1979). Silica and germania particles deposit by thermophoresis on the walls. The oxide mixture controls the refractive index of the light guide which enables light transport with minimal losses.

Thermophoretic sampling of aerosols

Studies of particle morphology and composition in reaction environments (e.g. combustors, aerosol reactors, flames) are important for process control and optimization. Dobbins *et al.* (1987) developed a technique which is based on the fact that soot deposition rates on cold targets immersed in flames are dominated by particle thermophoresis. The method is based on subjecting a cold probe surface for exposure times as short as 30 ms into a particle laden flame (e.g. sooting flame). Several thermophoretic probes exposed to the flames are examined by transmission electron microscopy (TEM) to reveal particle morphology. The morphological information provide not only valuable qualitative information on particle agglomeration, surface growth, and oxidation but also quantitative data on primary particle size as a function of reactor coordinates. Today, the thermophoretic sampling technique is routinely used in aerosol reactor characterization because the deposition rate does not depend on particle size and morphology for $Kn > 1$ (nanoparticles).

Thermophoretic film formation

Since the discovery of gas sensing effects on metal-oxide particles by Heiland (1957) these particles have found increasing use in applications spanning from toxic and explosive gas alarms to automotive sensors (Marek *et al.*, 2003). State-of-the-art gas sensors are generally fabricated using nanoparticles deposited as thick sensing films (Barsan *et al.*, 1999). However, conventional sensors suffer from serious technical limitations related to the way in which the nanoparticles are processed leading to significant variability of gas sensing performance, multiple and complex processing steps, and limited flexibility for multi-layer or functionalized configurations. Aerosol synthesis applying the Flame Spray Pyrolysis (FSP) technique (Mädler *et al.*, 2002) has been used for direct (in-situ) deposition of pure and functionalized (doped) sensing materials which eliminates these difficulties (Mädler *et al.*, 2006b). The direct thermophoretic deposition of nanoparticle agglomerates from the (hot) aerosol phase on the (cool) microelectronic chips results in fully formed functionalized sensing films (Fig. 13). These sensors are highly sensitive to carbon monoxide (CO).

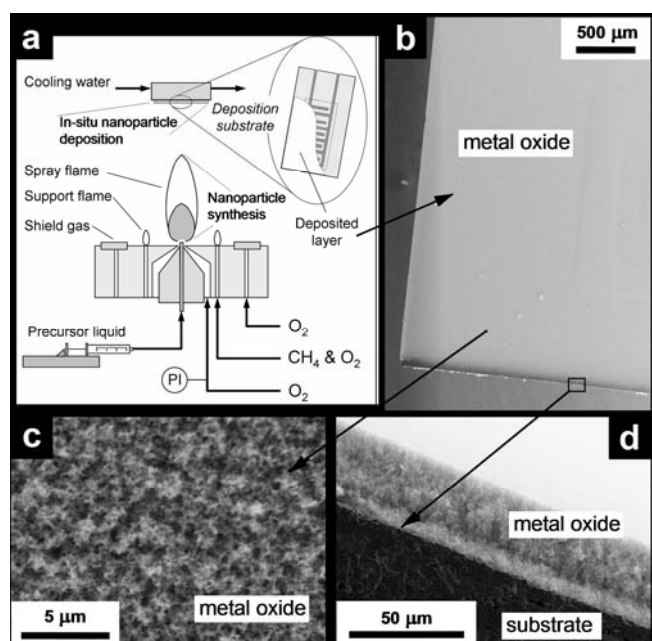


Fig. 13. Directly deposited sensing layers: a) Flame spray pyrolysis (FSP) apparatus for producing sensing nanoparticles that are directly deposited, forming sensing layers on a cooled substrate positioned above the flame. The inset graphic shows the sensor substrate with cutaway of the directly deposited sensor layer. b) SEM micrographs of a directly deposited SnO₂ sensing layer (deposition time of 180 s). c) High-magnification top-view of layer. d) Cross-sectional side view. Note the sensor layer thickness of $30 \pm 3 \mu\text{m}$ (Mädler *et al.*, 2006b).

Protection of lithographic masks against particle deposition

In the last few years the semiconductor industry uses thermophoresis as an effective tool to avoid “Light Point Defects” on wafers by particle deposition (Stratmann *et al.*, 1988; Peterson *et al.*, 1989; Ye *et al.*, 1991). Extreme ultraviolet (EUV) lithography will be introduced in 2009 to reduce the semiconductor feature size (Intel press release). To serve as a viable technology, particle contamination must be excluded from the lithographic mask. Traditional methods of lithographic mask protection, such as using organic membranes cannot be applied because the membrane absorbs too much EUV radiation and degrades under the EUV beam. Dedrick *et al.* (2005) developed a thermophoretic pellicle that protects the lithographic mask from particles using thermophoresis. Two requirements of the thermophoretic pellicle are: 1) the mask must be warmer than its surroundings and 2) the gas pressure must be sufficiently high to enable thermophoretic protection. Effective thermophoretic protection was reported for particles from 65 to 300 nm, over a wide range of gas pressures for temperature gradients as small as 2 – 15 K/cm.

3.2 Transport in electrical fields

Electric field forces which act on charged nanoparticles are commonly used in their filtration, production, classification and characterization.

3.2.1 Charging of nanoparticles

Nanoparticles suspended in a gas usually acquire some charges at the time of generation. Particle charging occurs when small ions attach to the particle surface. These ions can be generated by an external source such as a wire discharge or a radioactive source. In some cases particles charge themselves by heating to the point where they emit ions or electrons (thermoionic charging). Particles also attain a charge by radioactive decay of particle components (self charging). The charging is called bipolar in cases where the particles are charged with both polarities (positive and negative charged particles). If the particles are only charged with one polarity the charging is called unipolar. The number of acquired charges decreases with particle size. Bipolar charging of aerosols can be realized with a Kr_{85} radioactive source. The X-ray radiation ionizes the gas molecules which transfer the charge to the nanoparticle aerosol. Fig. 14 shows the fraction of particles with one and two units of positive charge after bipolar charging (Wiedensohler, 1988). Most of the nanoparticles remain uncharged. This poses a considerable difficulty for collection of nanoparticles by electrostatic precipitators. Higher charging efficiencies have been achieved with a corona charging. In this case only gas ions of one polarity (unipolar) are generated which will interact with the aerosol particles. Pui *et al.* (1988) have experimentally demonstrated that nearly 40% of 10-nm particles are charged for $n_i t$ values of the order of 10^7 ions s/cm^3 (n_i is the ion concentration and t the charging time).

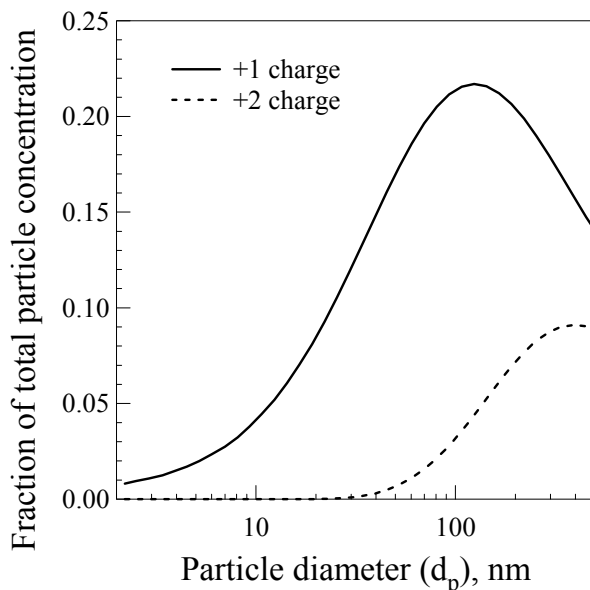


Fig. 14. Fraction of charged particles after passing through a bipolar charger. Only five percent of all particles smaller than 10 nm carry one positive charge. Particles larger than about 50 nm can also carry more than one charge while their fraction usually remains less than 10%.

3.2.2 Transport of nanoparticles in an electrical field

Charged nanoparticles are effectively transported in an electric field. The force on a particle carrying i elementary units of charge in an electrical field of strength E is given by:

$$F_{el} = i e E$$

where e is the elementary charge. When the electrical force is balanced by the drag force (Eq. 10) a steady migration velocity is obtained:

$$v_{el} = \frac{i e E}{\zeta}$$

Fig. 15 shows the steady state velocity of spherical singly charged nanoparticles. A 10 nm particle in an electric field of 2 kV/cm and 8 kV/cm has a migration velocity of 0.41 m/s and 1.64 m/s, respectively. These field strengths approximate the ones used in electrostatic precipitators (Friedlander, 2000). In comparison, an equivalent thermophoretic velocity of the same magnitude requires a large temperature gradient of $1.5 \cdot 10^6$ K/m. The high velocity of charged nanoparticles is advantageous in nanoparticle collection systems such as electret air filters. The electret in the filter possesses a permanent electric polarity (without external electrical field), analogous to a

permanent magnet. Charged particles are attracted by the electrical field force. This increases the collection efficiency and therefore the packing density of the collection fibers can be reduced which decreases the ventilation resistance of the filter - a key parameter in automotive cabin climate control.

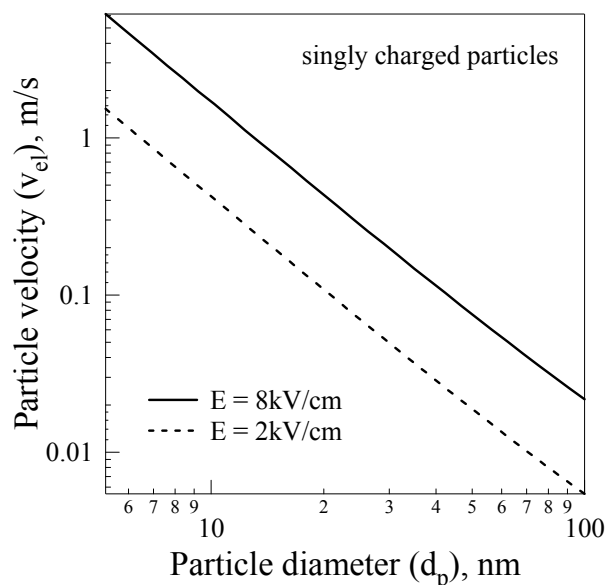


Fig. 15. Migration velocities of singly charged nanoparticles obtained under different electrical field strength (E). Small particles can obtain large migration velocities in electric fields once they successfully charged.

4. NANOPARTICLE TRANSPORT IN CONVECTIVE FLOWS

The transport of nanoparticles by the motion of the carrier gas is the predominant transport mechanism in the environment. Convective flows can lead to nanoparticle transport over hundreds of kilometers making their presence to a global effect world wide. The diffusional transport of the nanoparticles is always present and superimposed on the convective flow. This diffusional transport in flowing fluids is called convective diffusion. Additionally external force fields have major effects on particle motion. All three mechanisms (convection, diffusion, force fields) will affect the spatial particle concentration of a specific particle size with respect to time $n(x,y,z,t,d_p)$. The change in particle concentration is described by the following equation:

$$\frac{\partial n}{\partial t} + \mathbf{v} \cdot \nabla n = D \nabla^2 n - \nabla \cdot \mathbf{c}n \quad (31)$$

The values of the particle diffusion coefficient (D) and the particle migration velocity \mathbf{c} (e.g. thermophoretic velocity) are discussed in chapter (2) and chapter (3), respectively. The new quantity entering Eq. (31) is the gas velocity distribution, \mathbf{v} , which is determined by the fluid mechanical regime. In some cases, \mathbf{v} is obtained by solving the Navier-Stokes equation, but in most cases experimental data may be necessary. Solutions of Eq. (31) for specific applications and therefore specific boundary conditions are very well described by Friedlander (2000, chapter 3). This chapter is recommended for further reference on this topic.

5. SUMMARY

Transport of nanoparticles in gases differs from molecular transport. Nanoparticles are at least one order of magnitude larger than gas molecules which results in at least two orders of magnitude more surface area and three orders of magnitude more mass. Gas molecules interact with the nanoparticle surface area leading to momentum and heat transfer which translate into drag, Brownian motion and thermophoresis. The surface of nanoparticles is large enough to carry one or more charges which greatly influences their transport in electrical fields. The larger mass of nanoparticles leads to inertia effects such as persistence of Brownian velocity. Therefore, the mean free path of nanoparticles is larger than the gas mean free path. Nanoparticle sizes span over a size range of at least two orders of magnitude from 1 to 100 nm. For small nanoparticles (1 nm) their transport has similarities to molecular transport. However, as the size of the nanoparticle increases, momentum exchange with the gas molecules and nanoparticle inertia are different extending into the regime where corrections to the gas continuum model can be used. Nanoparticle agglomerates are the natural form of aerosol particles. Their transport properties in gases differ to that of spheres. Therefore, nanoparticle structure and morphology has to be taken into account in addition to their size. A key parameter for nanoparticle transport is the friction coefficient which was also presented for agglomerates. Nanoparticle transport is important in many applications ranging from aerosol sampling, nanoparticle film manufacture, light guide production, semiconductor protection etc.

ACKNOWLEDGEMENT

The work was supported by the UCLA Office of Instructional Development (OID). L.M. would like to thank the Deutsche Forschungsgemeinschaft DFG (German Research Foundation, Forschungsstipendium MA3333/1-1) for support. Stimulating discussions with Chui-sen Wang, Anshuman Amit Lall and Patrick Sislian are also gratefully acknowledged.

REFERENCES

- Bandyopadhyaya, R., Lall, A.A. and Friedlander, S.K. (2004). Aerosol Dynamics and the Synthesis of Fine Solid Particles. *Powder Technol.* 139(3): 193-199.
- Barsan, N., Schweizer-Berberich, M. and Gopel, W. (1999). Fundamental and Practical Aspects in the Design of Nanoscaled SnO₂ Gas Sensors: a Status Report. *Fresenius J. Anal. Chem.* 365(4): 287-304.
- Bird, R.B., Stewart, W.E. and Lightfoot, E.N. (2002). *Transport Phenomena*, John Wiley & Sons, Inc., New York.
- Brenner, H. (2005a). Kinematics of Volume Transport. *Physica A.* 349(1-2): 11-59.
- Brenner, H. (2005b). Navier-Stokes Revisited. *Physica A.* 349(1-2): 60-132.
- Brock, J.R. (1962). On the Theory of Thermal Forces Acting on Aerosol Particles. *J. Colloid. Sci.* 17(8): 768-780.
- Brown, R. (1866). A Brief Account of Microscopical Observations Made in the Months of June, July and August, 1827, on the Particles Contained in the Pollen of Plants; and on the General Existence of Active Molecules in Organic and Inorganic Bodies. The miscellaneous botanical works of Robert Brown, J. J. Bennett, ed., R. Hardwicke, London, 464-486.
- Chan, P. and Dahneke, B. (1981). Free-molecule Drag on Straight Chains of Uniform Spheres. *J. Appl. Phys.* 52(5): 3106-3110.
- Chandrasekhar, S. (1943). Stochastic Problems in Physics and Astronomy. *Rev. Mod. Phys.* 15(1): 1-89.
- Chapman, S. and Cowling, T.G. (1958). *The Mathematical Theory of Non-Uniform Gases*, Cambridge University Press, London.
- Dahneke, B. (1973). Slip Correction Factors for Nonspherical Bodies - II Free molecular Flow. *J. Aerosol Sci.* 4: 147-161.
- Dahneke, B. (1982). Viscous Resistance of Straight-chain Aggregates of Uniform Spheres. *Aerosol Sci. Technol.* 1(2): 179-185.
- Davies, C.N. (1945). Definitive Equations for the Fluid Resistance of Spheres. Proceedings of the Physical Society of London. 57(322): 259-270.
- de Gennes, P.G. (1988). *Scaling Concepts in Polymer Physics*, Cornell University Press, London.
- Dedrick, D.E., Beyer, E.W., Rader, D.J., Klebanoff, L.E. and Leung, A.H. (2005). Verification Studies of Thermophoretic Protection for Extreme Ultraviolet Masks. *J. Vac. Sci. Technol. B.* 23(1): 307-317.
- Dobbins, R.A. and Megaridis, C.M. (1987). Morphology of Flame-generated Soot as Determined by Thermophoretic Sampling. *Langmuir.* 3(2): 254-259.
- Einstein, A. (1905). Investigations on the Theory of the Brownian Movement. *Annalen der Physik.* 17: 549.

- Epstein, P.S. (1924). On the Resistance Experienced by Spheres in their Motion Through Gases. *Phys. Rev.* 23: 710-733.
- Filippov, A.V. (2001). Phoretic Motion of Arbitrary Clusters of N Spheres. *J. Colloid Interface Sci.* 241(2): 479-491.
- Filippov, A.V., Zurita, M. and Rosner, D.E. (2000). Fractal-like Aggregates: Relation Between Morphology and Physical Properties. *J. Colloid Interface Sci.* 229(1): 261-273.
- Friedlander, S.K. (2000). *Smoke, Dust, and Haze: Fundamentals of Aerosol Dynamics*, Oxford University Press, New York.
- Fuchs, N.A. (1964). *The Mechanics of Aerosols*, Pergamon, Oxford.
- Gallis, M.A., Rader, D.J. and Torczynski, J.R. (2004). A Generalized Approximation for the Thermophoretic Force on a Free-molecular Particle. *Aerosol Sci. Technol.* 38(7): 692-706.
- Gallis, M.A., Torczynski, J.R. and Rader, D.J. (2001). An Approach for Simulating the Transport of Spherical Particles in a Rarefied Gas Flow via the Direct Simulation Monte Carlo Method. *Phys. Fluids.* 13(11): 3482-3492.
- Gleiter, H. (1989). Nanocrystalline Materials. *Prog. Mater Sci.* 33(4): 223-315.
- Heiland, G. (1957). Zum Einfluss von Wasserstoff auf die Elektrische Leitfähigkeit an Der Oberfläche von Zinkoxydkristallen. *Z. Phys.* 148(1): 15-27.
- Hinds, W.C. (1999). *Aerosol Technology*, John Wiley & Sons, Inc. New York.
- Hirschfelder, J.O., Curtiss, C.F. and Bird, R.B. (1964). *Molecular Theory of Gases and Liquids*, John Wiley & Sons, Inc., New York.
- Ivchenko, I.N. and Yalamov, Y.I. (1971). Hydrodynamic Method for Calculation of Rate of Thermophoresis of Moderately Large Involatile Aerosol Particles. *Russ. J. Phys. Chem, USSR.* 45(3): 317-319.
- Kaer, S.K., Rosendahl, L.A. and Baxter, L.L. (2006). Towards a CFD-based Mechanistic Deposit Formation Model for Straw-fired Boilers. *Fuel.* 85(5-6): 833-848.
- Kammler, H.K., Mädler, L. and Pratsinis, S.E. (2001). Flame Synthesis of Nanoparticles. *Chem. Eng. Technol.* 24(6): 583-596.
- Kirkwood, J.G. and Riseman, J. (1948). The Intrinsic Viscosities and Diffusion Constants of Flexible Macromolecules in Solution. *J. Chem. Phys.* 16(6): 565-573.
- Kodas, T.T. and Hampden-Smith, M.J. (1999). *Aerosol Processing of Materials*, Wiley-VCH, New York.
- Lall, A.A. and Friedlander, S.K. (2006). On-line Measurement of Ultrafine Aggregate Surface area and Volume Distributions by Electrical Mobility Analysis: I. Theoretical Analysis. *J. Aerosol Sci.* 37(3): 260-271.
- Li, Z.G. and Wang, H. (2003a). Drag Force, Diffusion Coefficient, and Electric Mobility of Small Particles. I. Theory Applicable to the Free-molecule Regime. *Phys. Rev. E.* 68(6): 061206-1 - 061206-9.

- Li, Z.G. and Wang, H. (2003b). Drag Force, Diffusion Coefficient, and Electric Mobility of Small particles. II. Application. *Phys. Rev. E.* 68(6): 061207-1 - 061207-13.
- Mackowski, D.W. (1990). Phoretic Behavior of Asymmetric Particles in Thermal Nonequilibrium with the Gas - 2-sphere Aggregates. *J. Colloid Interface Sci.* 140(1): 138-157.
- Mackowski, D.W. (2006). Monte Carlo Simulation of Hydrodynamic Drag and Thermophoresis of Fractal Aggregates of Spheres in the Free-molecule Flow Regime. *J. Aerosol Sci.* 37(3): 242-259.
- Mädler, L., Kammler, H.K., Mueller, R. and Pratsinis, S.E. (2002). Controlled Synthesis of Nanostructured Particles by Flame Spray Pyrolysis. *J. Aerosol Sci.* 33(2): 369-389.
- Mädler, L., Lall, A.A. and Friedlander, S.K. (2006a). One-step Aerosol Synthesis of Nanoparticle Agglomerate Films: Simulation of Film Porosity and Thickness. *Nanotechnology.* 17(19): 4783-4795.
- Mädler, L., Roessler, A., Pratsinis, S.E., Sahm, T., Gurlo, A., Barsan, N. and Weimar, U. (2006b). Direct Formation of Highly Porous Gas-sensing Films by in-situ Thermophoretic Deposition of Flame-made Pt/SnO₂ Nanoparticles. *Sens. Actuators. B Chem.* 114(1): 283-295.
- Marek, J., Trah, H.P., Suzuki, Y. and Yokomori, I. (2003). *Sensors for Automotive Technology*, VCH: Weinheim.
- Nazaroff, W.W., Ligocki, M.P., Ma, T. and Cass, G.R. (1990). Particle Deposition in Museums - Comparison of Modeling and Measurement Results. *Aerosol Sci. Technol.* 13(3): 332-348.
- Osterwalder, N., Capello, C., Hungerbühler, K. and Stark, W.J. (2006). Energy Consumption During Nanoparticle Production: How Economic is Dry Synthesis. *J. Nanopart. Res.* 8(1): 1-9.
- Peterson, T.W., Stratmann, F. and Fissan, H. (1989). Particle Deposition on Wafers - a Comparison Between 2 Modeling Approaches. *J. Aerosol Sci.* 20(6): 683-693.
- Pui, D.Y.H., Fruin, S. and McMurry, P.H. (1988). Unipolar Diffusion Charging of Ultrafine Aerosols. *Aerosol Sci. Technol.* 8(2): 173-187.
- Rogak, S.N., Flagan, R.C. and Nguyen, H.V. (1993). The Mobility and Structure of Aerosol Agglomerates. *Aerosol Sci. Technol.* 18(1): 25-47.
- Rouse, P.E. (1953). A Theory of the Linear Viscoelastic Properties of Dilute Solutions of Coiling Polymers. *J. Chem. Phys.* 21(7): 1272-1280.
- Rudiyak, V.Y. and Krasnolutski, S.L. (2001). Kinetic Description of Nanoparticle Diffusion in Rarefied Gas. *Doklady Phys.* 46(12): 897-899.
- Seinfeld, J.H. and Pandis, S.N. (1998). *Atmospheric Chemistry and Physics: From air Pollution to Climate Change*, John Wiley & Sons, Inc. New York.
- Simpkins, P.G., Greenberg-Kosinski, S. and MacChesney, J.B. (1979). Thermophoresis - mass-transfer Mechanism in Modified Chemical Vapor-deposition. *J. Appl. Phys.* 50(9): 5676-5681.
- Stratmann, F., Fissan, H., Papperger, A. and Friedlander, S. (1988). Suppression of Particle Deposition to Surfaces by the Thermophoretic Force. *Aerosol Sci. Technol.* 9(2): 115-121.

- Talbot, L., Cheng, R.K., Schefer, R.W. and Willis, D.R. (1980). Thermophoresis of Particles in a Heated Boundary-layer. *J. Fluid Mech.* 101(DEC): 737-758.
- Tandon, P. and Rosner, D.E. (1995). Translational Brownian Diffusion-Coefficient of Large (Multiparticle) Suspended Aggregates. *Ind. Eng. Chem.* 34(10): 3265-3277.
- Tsantilis, S. and Pratsinis, S.E. (2004). Soft- and Hard-agglomerate Aerosols made at High Temperatures. *Langmuir.* 20(14): 5933-5939.
- Tyndall, J. (1870). On Dust and Disease. Proceedings Royal Institution of Great Britain, 6: 1-14.
- Virtanen, A., Ristimäki, J. and Keskinen, J. (2004). Method for measuring effective density and fractal dimension of aerosol agglomerates. *Aerosol Sci. Technol.* 38(5): 437-446.
- Waldmann, L. and Schmitt, K.H. (1966). *Thermophoresis and Diffusiophoresis of Aerosols*. Aerosol Science, C.N. Davies, ed., Academic Press Inc., London. p.137-162.
- Walsh, J.K., Weimer, A.W. and Hrenya, C.M. (2006). An Experimental Study of Thermophoretic Deposition of Aerosol Particles in Laminar Tube Flow with Mixed Convection. *Aerosol Sci. Technol.* 40(3): 178-188.
- Wang, C., Friedlander, S.K. and Mädler, L. (2005). Nanoparticle Aerosol Science and Technology: An Overview. *Particuology.* 3(5): 243-254.
- Weber, A.P. and Friedlander, S.K. (1997). In Situ Determination of the Activation Energy for Restructuring of Nanometer Aerosol Agglomerates. *J. Aerosol Sci.* 28(2): 179-192.
- Weimer, A.W., Cochran, G.A., Eisman, G.A., Henley, J.P., Guiton, T.A., Knudsen, A.K. and Nicholas, N.R. (1993). Controlling Thermophoresis in the Exothermic Nitridation of an Aluminum Aerosol. *Aerosol Sci. Technol.* 19(4): 491-498.
- Wiedensohler, A. (1988). An Approximation of the Bipolar Charge-distribution for Particles in the Sub-micron Size Range. *J. Aerosol Sci.* 19(3): 387-389.
- Willeke, K. (1976). Temperature Dependence of Particle Slip in a Gaseous Medium. *J. Aerosol Sci.* 7: 381-387.
- Ye, Y., Pui, D.Y.H., Liu, B.Y.H., Opiolka, S., Blumhorst, S. and Fissan, H. (1991). Thermophoretic Effect of Particle Deposition on a Free Standing Semiconductor Wafer in a Clean room. *J. Aerosol Sci.* 22(1): 63-72.
- Zheng, F. (2002). Thermophoresis of Spherical and Non-spherical Particles: A Review of Theories and Experiments. *Adv. Colloid Interface Sci.* 97(1-3): 255-278.
- Zurita-Gotor, M. (2006). Size- and Structure-independence of the Thermophoretic Transport of an Aerosol Particle for Specular Boundary Conditions in the free Molecule Regime. *J. Aerosol Sci.* 37(3): 283-291.

Received for review, March 16, 2007

Accepted, May 14, 2007